Alloy clustering and defect structure in the molecular beam epitaxy of $In_{0.53}Ga_{0.47}As$ on silicon

Alexandros Georgakilas[a] and Athanasios Dimoulas
Institute of Electronic Structure and Laser, Foundation for Research and Technology–Hellas (FORTH), P.O. Box 1527, 711 10 Heraklion, Crete, Greece

Aristotelis Christou
Institute of Electronic Structure and Laser, Foundation for Research and Technology–Hellas (FORTH), P.O. Box 1527, 711 10 Heraklion, Crete, Greece, and CALCE Electronic Packaging Research Center, Microelectronics Devices Laboratory, University of Maryland, College Park, Maryland 20742

John Stoemenos
Physics Department, Aristotle University of Thessaloniki, 540 06 Thessaloniki, Greece

(Received 18 November 1991; accepted 7 February 1992)

The MBE growth of $In_xGa_{1-x}As$ ($x \sim 0.53$) on silicon substrates has been investigated emphasizing the effects of substrate orientation and buffer layers between $In_{0.53}Ga_{0.47}As$ and Si. It is shown that growth on silicon substrates misoriented from (001) toward a [110] direction eliminates the presence of antiphase domains. The best $In_{0.53}Ga_{0.47}As$ surface morphology was obtained when a 0.9 μm epitaxial Si buffer was initially grown, followed by a pre-exposure of the silicon surface to As_4 at 350 °C, followed by the growth of $In_{0.53}Ga_{0.47}As$. Threading dislocations, stacking faults, low-angle grain boundaries, and spinodal decomposition were observed by TEM in the InGaAs layers. The spinodal contrast scale was shown to depend on the buffer type and the total InGaAs thickness. Thick buffers consisted of GaAs or graded $In_xGa_{1-x}As$ layers, and large $In_{0.53}Ga_{0.47}As$ thicknesses favor the development of a coarse-scale spinodal decomposition with periodicity around 0.1 μm. Thin GaAs buffers or direct $In_{0.53}Ga_{0.47}As$ growth on Si may result in a fine-scale decomposition of periodicity ~10 nm. The principal strain direction of the spinodal decomposition appeared along the $[1\bar{1}0]$ direction, parallel to the vicinal Si surface step edges. InGaAs immiscibility affects the InGaAs growth process, favoring a 3-D growth mode. X-ray diffraction measurements and photoreflectance spectra indicated that the sample quality was improved for samples exhibiting a fine-scale spinodal decomposition contrast even if they contained a higher dislocation density. Threading dislocations run almost parallel to the [001] growth axis and are not affected by strained layers and short period $(InAs)_3/(GaAs)_3$ superlattices. The lowest double crystal diffractometry FWHM for the (004) InGaAs reflection was 720 arc sec and has been obtained growing InGaAs directly on Si, while the lowest dislocation density was 3×10^9 cm^{-2} and was obtained using a 1.5 μm GaAs buffer before the $In_{0.53}Ga_{0.47}As$ deposition.

I. INTRODUCTION

The heteroepitaxy of III-V semiconductors on Si substrates has been stimulated by the potential for monolithic integration of III-V high-speed and optical components with the advanced Si circuitry. A significant improvement has taken place in the epitaxy of GaAs on Si and our investigations indicated that the GaAs/Si properties are within 10% of the homoepitaxial material grown under similar conditions.[1] Such material has resulted in the fabrication of transistors and photodetectors.[1–3] The fabrication of long-life lasers remains a problem[4] due to the high threading dislocation density[3] of 10^8 cm^{-2} and the residual thermal stress of 10^9 dyn/cm^2 that exist in the GaAs epilayers.[5]

The epitaxy of $In_xGa_{1-x}As$ on Si is also very interesting, specifically since it presents the possibility of integrating optical devices with wavelengths of 1.3–1.55 μm, appropriate for low loss communication through optical fibers. However, for In composition close to 0.53 ($\lambda = 1.65$ μm) a large lattice misfit, $f = -0.075$, occurs between InGaAs and Si. Thus, the heteroepitaxy of InGaAs on Si in addition to the problems of "polar on nonpolar" growth (i.e., antiphase

[a]Present address: Visiting researcher in the CALCE Electronic Packaging Research Center, Microelectronics Devices Laboratory, University of Maryland, College Park, Maryland 20742.

domain[6,7] formation) must overcome the significantly higher misfit that exists in comparison to GaAs on Si. Antiphase domains (APDs) in the zinc blende lattice are the domains that consist of material volumes with the inverse occupation of each sublattice. Alloy clustering may also appear in the ternary InGaAs epilayers due to the mixing of two lattice mismatched binaries (InAs, GaAs). Indeed, immiscibility is predicted for the $In_xGa_{1-x}As$ alloys under a range of specific conditions (composition and temperature).[8–12]

The heteroepitaxy of lattice mismatched thin films on various substrates involves many difficulties. A network of misfit dislocations should be formed, ideally, at the epilayer-substrate interface in order to accommodate the lattice misfit.[13] However, it is well known that many other defects are also generated,[14–17] such as stacking faults, microtwins, and threading dislocations, which propagate in the overlayers, thus degrading their crystal quality. Their origin has been attributed to the initial 3-D growth mode[15–17] and to the generation mechanism of misfit dislocations by half loops that nucleate on the film surface and expand to the interface.[14] Generally a 3-D growth mode is predicted to be energetically favored for the deposition of films that are lattice mismatched to their substrates.[16,18]

Composition variations in In based III-V ternary and quaternary epitaxial layers have been observed by TEM and STEM examination and have been recently reviewed.[19,20] In most cases, composition inhomogeneities have been reported in InGaAsP layers grown by LPE and there is little information concerning inhomogeneities in the MBE grown InGaAs on (001) GaAs or InP.[21,22] The composition modulation is attributed to spinodal decomposition and has mainly shown two types of quasi-periodic contrast modulation in TEM images for various III-V alloy films, a fine-scale speckle contrast with a period of ~15 nm and a coarse-scale contrast with a period of ~125 nm. In both cases, the modulations are oriented approximately along the ⟨100⟩ directions in the (001) film surface plane, and a basket-weave contrast appears for the coarse modulation. A controversy still exists about which contrast scales are actually related to composition modulations,[19,20] but evidence indicates that both contrast scales are related to composition nonuniformity.[22–25] The III-V ternaries with composition variations are expected to have inferior electrical and optical properties. However, alloy clustering may resist the degradation of light-emitting devices[20] through some type of strengthening mechanism. Therefore, the epitaxial InGaAs/InAlAs layers on silicon may prove appropriate for the fabrication of reliable light sources.

Despite the large lattice misfit, $f = -0.075$, the first attempts to grow InP[26,27] and $In_xGa_{1-x}As$,[28,29] with $x = 0.53$, on silicon were carried out. In order to avoid the growth of phosphorous-containing compounds, the present investigation is limited to the growth of InGaAs on silicon. The experiments were aimed at understanding the highly mismatched system of InGaAs/Si and at determining the optimum growth conditions for the InGaAs structures.

Threading dislocations, stacking faults, low-angle grain boundaries, and spinodal decomposition were observed in the $In_{0.53}Ga_{0.47}As$ films. The high defect densities are not related to the lattice misfit but rather to the 3-D growth mode of InGaAs which is favored by the InGaAs alloy trend toward immiscibility. The spinodal contrast modulation occurred perpendicular to the [110] silicon vicinal direction, contrary to previous observations[19–25] which report contrast modulation along the [100] and [010] directions on the (001) plane. The scale of the spinodal decomposition contrast is shown to depend on the buffer layer type and the total $In_{0.53}Ga_{0.47}As$ thickness. InGaAs grown directly on silicon exhibited better optical properties, although a lower defect density was obtained in a structure having a 1.5 μm GaAs intermediate layer. This observation may be related to the fine-scale contrast observed in the samples without a GaAs intermediate layer. A coarse-scale contrast modulation was observed in samples with the 1.5 μm GaAs intermediate layer.

II. EXPERIMENTAL

The InGaAs on Si samples were grown in a dual deposition chamber MBE system which combines both III-V and Si deposition chambers. We examined Si substrates with (001) orientations, on axis, misoriented 4° toward [100] and misoriented 3°–4° toward [110]. The substrates were p-type with resistivity of 80–200 Ω cm. They were initially degreased in boiled TCE, acetone, propan-2-ol, and rinsed in running de-ionized water (D.I.). Then, they were etched for 10 min in $HF:H_2O$ (1 : 10) and 10 min in hot $HNO_3:H_2O$ (1 : 1), rinsed in running D.I., dried with N_2, and loaded into the MBE system utilizing indium-free holders. This chemical preparation produces a thin volatile oxide on the Si surface to protect it from carbon contamination.

The Si oxide desorption was accomplished by heating either in the III-V chamber at ~850–900 °C for 10 min, or in the Si chamber at 750 °C for 10 min under a low Si flux. The low Si flux assists the oxide desorption by the reaction of Si atoms with SiO_2, resulting in the volatile SiO product.[30] Thus, it was possible to reduce more than 100 °C the heating temperature for the desorption of Si oxide. The latter desorption procedure is compatible to the thermal tolerances of preprocessed silicon substrates and hence to monolithic integration. The Si cleaning was monitored by RHEED (Reflection High Energy Electron Diffraction) observa-

tions while RHEED was also used to monitor the various growth steps.

The general InGaAs on Si sample structure is shown in Fig. 1. The III-V layer deposition always started by the pre-exposure of the Si surface to As_4 at ~700 °C or ~350 °C for 1 min. A two-step[1] GaAs initial layer growth with thickness of 30 nm up to 1.5 μm was investigated as an intermediate layer before the InGaAs deposition. In other samples, InGaAs was grown directly on Si. Additionally, we also examined intermediate 0.9 μm thick Si buffer layers grown on Si (Si chamber) before the InGaAs layers. Abruptly or continuously compositionally graded InGaAs buffer layers and $(InAs)_3/(GaAs)_3$ short period superlattices were investigated scoping at the prevention of the threading dislocation propagation. The total InGaAs thickness was varied from 0.7 μm to 6.0 μm. The As_4 beam flux equivalent pressure was 2×10^{-5} Torr, the InGaAs growth rate 1.0 μm/h, and the substrate temperature ~500 °C.

The structure parameters of the various samples grown on Si substrates misoriented from (001) 3°–4° toward the [110] direction are described in Table I. Three different buffer layer types were used and their structure is given subsequently (starting from the first layers below the final $In_{0.53}Ga_{0.47}As$ film):

I: /0.2 μm $In_{0.44}Ga_{0.56}As$/0.2 μm $In_{0.35}Ga_{0.65}As$/10 periods of {10 nm $In_{0.20}Ga_{0.80}As$/10 nm GaAs}/

II: /10 periods of {10 nm $In_yAl_{1-y}As$/10 nm $In_{(y+0.1)}Al_{(0.9-y)}As$} repeated sequentially for y: 0.4, 0.3, 0.2, 0.1, 0/

III: /0.8 μm $In_xGa_{1-x}As$, x graded continuously from $x = 0.51$ to 0.53/0.2 μm $In_{0.51}Ga_{0.49}As$/25 nm $In_{0.50}Ga_{0.50}As$/.

The structural quality of InGaAs on Si was characterized by Double Crystal X-rays Diffractometry (DDX), Scanning Electron Microscopy (SEM), and Transmission Electron Microscopy, both in planar (TEM) and cross-sectional (XTEM) film geometries. Photoreflectance spectroscopy (PR)[5] at room temperature was used to assess the optical quality of the layers. The FWHM values of DDX (004) reflections for InGaAs were determined for the various samples. The SEM was used to observe the InGaAs surface morphologies, while Electron Channeling Patterns (ECPs) were also obtained in the SEM microscope. The XTEM specimens were prepared using conventional mechanical and Ar ion thinning methods. For the TEM observations (001) planar specimens were prepared using back chemical etching of the substrate combined with a final ion thinning step.

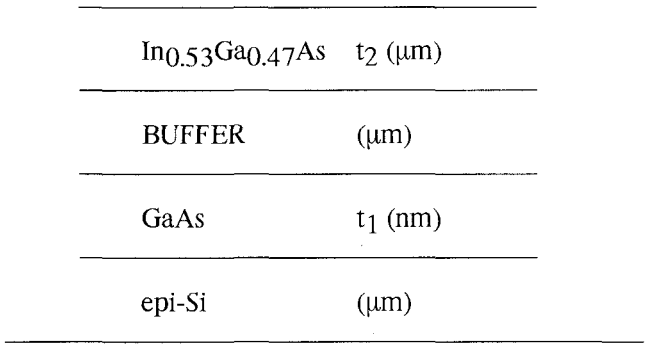

FIG. 1. Schematic illustration of the general $In_{0.53}Ga_{0.47}As$ on Si structure.

III. RESULTS

The substrate oxide desorption resulted in Si surfaces exhibiting a bright double 2×1 domain RHEED pattern. When a 0.9 μm thick Si buffer was grown, the Si surface reconstruction remained similar except for the appearance of streak splitting, indicating that a periodic step array was formed on the Si surface. The Si deposition improves the Si surface quality which initially contains surface defects and probably facets.[31] Thus, a homogeneous nucleation can be succeeded on the improved Si surface resulting in a 2-D growth mode from the early stages of growth. The GaAs grown on Si with an intermediate Si buffer exhibited absolutely smooth surfaces [Fig. 2(b)]. Similarly, the best InGaAs on Si morphology was obtained for InGaAs grown directly on a 0.9 μm Si buffer [Fig. 2(a)]. In both cases the Si surface was pre-exposed to As_4 at 350 °C. However, as is shown in Figs. 2(a) and 2(b), the InGaAs on Si surface morphology is significantly inferior to the absolutely smooth GaAs on Si surface obtained under the same growth conditions. Thus, it seems that a rough growth front occurred throughout the entire InGaAs film deposition, in contrast to GaAs on Si, where a 2-D growth occurs from the very early stages of growth.[32]

The InGaAs films exhibited very rough surface morphologies for Si substrates misoriented from (001) 4° toward [100] [Fig. 2(c)]. These surfaces exhibited a complicated faceted structure similar to GaAs on Si samples (for the same orientation), and this is attributed to the APD structure on that orientation.[7] Better surface morphologies were obtained for misorientation toward [110] [Fig. 2(a)]. The surface roughness is aligned parallel to the [110] direction, indicating that APDs were effectively suppressed. An APD structure appeared also for Si substrates oriented exactly along (001). Thus, we chose to use substrates misoriented in a [110] zone for the remainder of the experiments (Table I).

The DDX rocking curve FWHM for the (004) InGaAs reflection are shown in Table I for the various samples grown on Si (001) 3°–4° off toward [110]. The samples #1–7 have only an intermediate GaAs

TABLE I. DDX FWHM of the (400) reflection of InGaAs on Si. The general sample structure is shown in Fig. 1, while the various buffer types are described in the text.

Sample no.	epi-Si (μm)	Buffer type	GaAs t_1 (nm)	$In_{0.53}Ga_{0.47}As$ t_2 (μm)	$In_{0.53}Ga_{0.47}As$ FWHM (arc sec)
1	...	...	30	2.2	1550
2	...	...	30	3.7	1100–1290
3	...	...	30	3.7	1000–1180
4	...	...	40	3.7	1250
5	...	...	30	3.7	900–1100
6	...	...	160	4.5	1220
7	...	...	1500	3.6	1240
8	...	I (0.6 μm)	50	2.5	1500
9	...	I (0.6 μm)	50	2.8	1220
10	...	I (0.6 μm)	1500	2.5	1320
11	...	II (1.0 μm)	40	3.0	1460
12	0.9	III (1.0 μm)	...	2.0	720
13	0.9	III (1.0 μm)	...	2.0	790
14	...	...	...	6.0	870

layer. It is clearly evident that the FWHM is nearly independent of the GaAs thickness. The lower value of 900 arc sec appears for the sample with a thin 30 nm GaAs intermediate layer. The optimum thicknesses for this structure are estimated to be $t_2 = 3.5$ μm and $t_1 =$ 30 nm. The graded buffer layers of types I and II do not seem to improve drastically the $In_{0.53}Ga_{0.47}As$ quality, while type I buffer is better than type II.

The lowest FWHM values were obtained when InGaAs was grown directly on Si. For sample #12 (FWHM = 720 arc sec), initially 25 nm $In_{0.50}Ga_{0.50}As$ was grown on Si at 350 °C. The layer was annealed at 500 °C for 5 min, and 0.2 μm $In_{0.51}Ga_{0.49}As$ was grown at 500 °C. Subsequently, a 0.8 μm $In_xGa_{1-x}As$ layer was grown with x continuously graded from 0.51 to 0.53. Finally, a 2 μm $In_{0.53}Ga_{0.47}As$ was grown. The above described InGaAs composition grading was also used in #13. For both of these two samples a 0.9 μm Si buffer was grown on the substrate before the InGaAs deposition (Table I). Comparing #12 and #13 with #14 (without Si buffer), the advantage offered by Si buffer layers is clearly evident.

Photoreflectance spectroscopy (PR) measurements at 300 K have been taken from several of our samples shown in Table I. The best PR spectrum was obtained for sample #12 and it is shown in Fig. 3. The spectrum

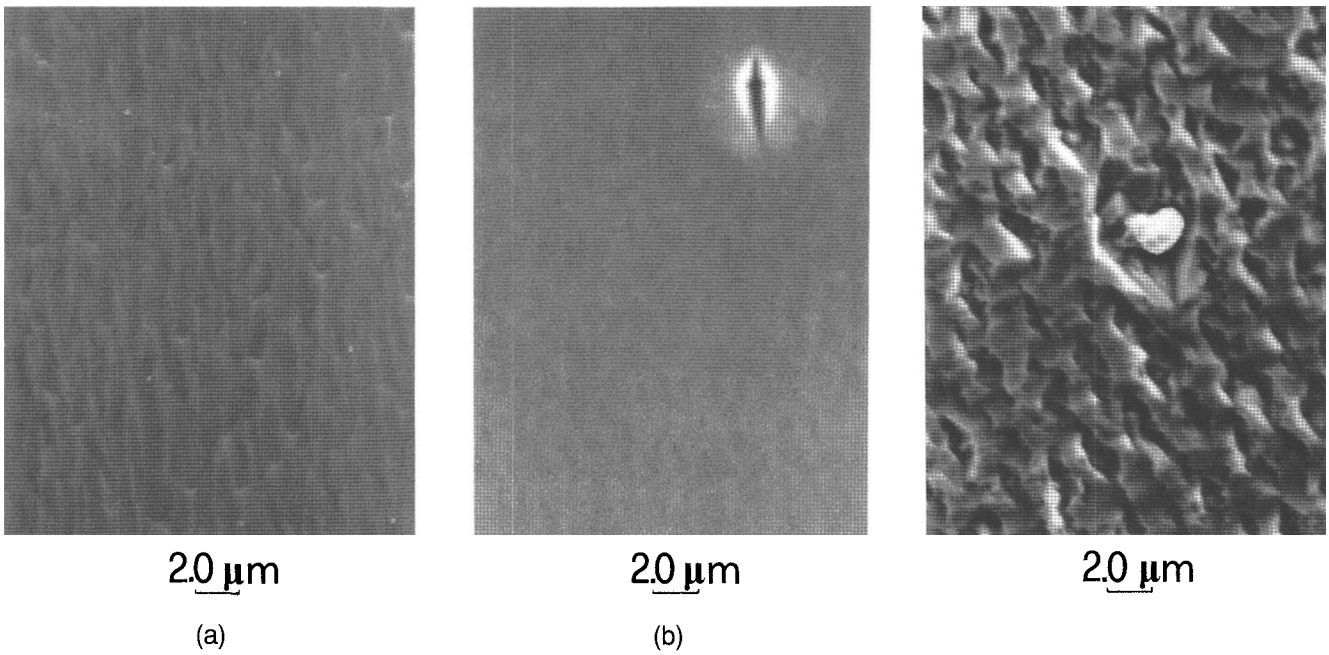

FIG. 2. SEM micrographs showing the surface morphologies obtained in (a) 2 μm $In_{0.53}Ga_{0.47}As$/0.9 μm Si/Si and (b) 2 μm GaAs/0.35 μm Si/Si, for Si substrate orientation (001) 4° off toward [110], and (c) 3 μm $In_{0.53}Ga_{0.47}As$ on Si (001) 4° off toward [100].

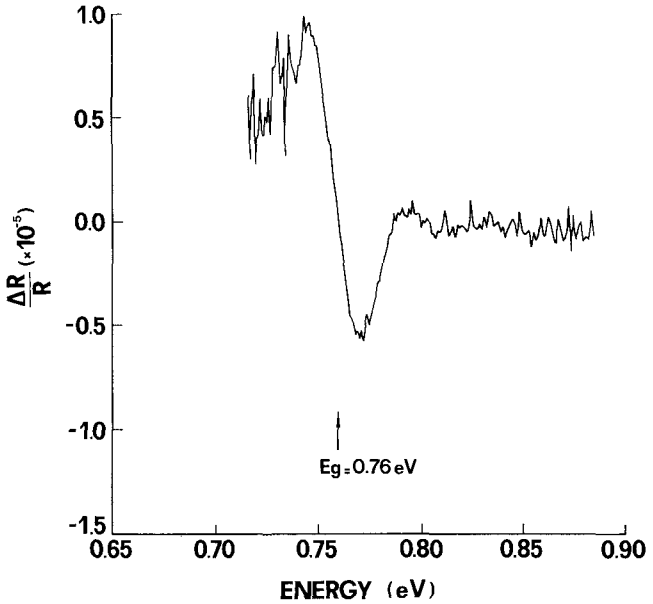

FIG. 3. The best photoreflectance spectrum at 300 K, obtained for sample #12.

intensity and broadening compare well with moderate quality lattice matched InGaAs on InP samples.

The main crystal defects observed by TEM and XTEM observations in the $In_xGa_{1-x}As$ films are threading dislocations, low-angle grain boundaries, stacking faults, and spinodal decomposition (Figs. 4–10). Five samples were characterized and the results are tabulated in Table II. The defect densities shown in Table II for samples #7, 9, 12, and 14 have been deduced from TEM observations of (001) planar specimens near the $In_{0.53}Ga_{0.47}As$ surface. The surface roughness was estimated from XTEM observations, and thus there is no value for #9 which was examined only by TEM. Sample #1 was examined only in XTEM which could not reveal the low-angle boundaries. We can approximate a dislocation density near the InGaAs surface

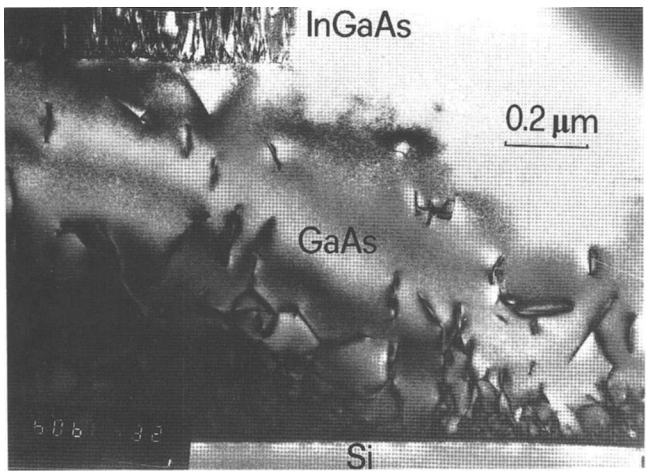

FIG. 4. XTEM micrograph showing the GaAs/Si and $In_{0.53}Ga_{0.47}As$/GaAs interfaces in sample #7.

only, while stacking fault density approximations are not possible.

The majority of the dislocations are threading dislocations running almost perpendicular to the surface. The lowest (3×10^9 cm^{-2}) dislocation density is present near the surface. At larger depths of the InGaAs, the dislocation density approaches the value of 10^{11} cm^{-2}. The generation mechanism of these large dislocation densities is related to the InGaAs growth mode and not to the lattice misfit value. This is clearly evident in Figs. 4 and 5. In Fig. 4 both the GaAs/Si and InGaAs/GaAs interfaces of sample #7 are shown. Each interface is shown in higher magnification in the micrographs of Figs. 5(a) and 5(b), respectively. Although the InGaAs/GaAs interface [Fig. 5(b)] exhibits a lower misfit and does not consist of polar on nonpolar growth,[6] the defect density is significantly higher compared to the GaAs/Si interface [Fig. 5(a)]. In addition, the XTEM micrograph of the GaAs/Si interface shows periodic rows of misfit dislocations with spacing 9 nm and does not show a periodic contrast due to misfit dislocations at the InGaAs/GaAs interface.

Planar view micrographs from the InGaAs/GaAs interface have shown very irregular moiré patterns and misfit dislocation networks (Fig. 6). The irregularities in moiré patterns indicate that a 3-D nucleation occurred with slightly different orientation for various nuclei. Segments of misfit dislocations were observed, denoted by the letter A in Figs. 6(a) and 6(b), which is also consistent with the 3-D nucleation. The mean length of the segments is about 100 nm. For each misfit dislocation segment a contribution of two threading dislocations is expected.

The XTEM micrograph of Fig. 7(a) shows the interfacial region of sample #12. The InGaAs film was grown directly on Si by a two-step-like process, as described earlier in the text. It is clearly evident that a high defect density has been localized in the low temperature 25 nm $In_{0.50}Ga_{0.50}As$ nucleation layer. An abrupt InGaAs/Si interface is shown and periodic rows of misfit dislocations with spacing 5.2 nm are observed [Fig. 7(a)]. However, TEM observations [Fig. 7(b)] have shown that the dislocation density near the $In_{0.53}Ga_{0.47}As$ surface was 7×10^9 cm^{-2}, higher than the value of 3×10^9 cm^{-2} that was obtained for sample #7 (Table II). In addition, the XTEM observations indicated that the type III buffer does not prevent the propagation of threading dislocations, and some improvement is obtained only in the first two steps of 25 nm $In_{0.50}Ga_{0.50}As$/0.2 μm $In_{0.51}Ga_{0.49}As$.

XTEM micrographs for sample #1 grown with a very thin 30 nm GaAs buffer also indicated a high dislocation density similar to the previous samples. In addition, a higher surface roughness appeared for #1 which is attributed to the lower total GaAs thickness

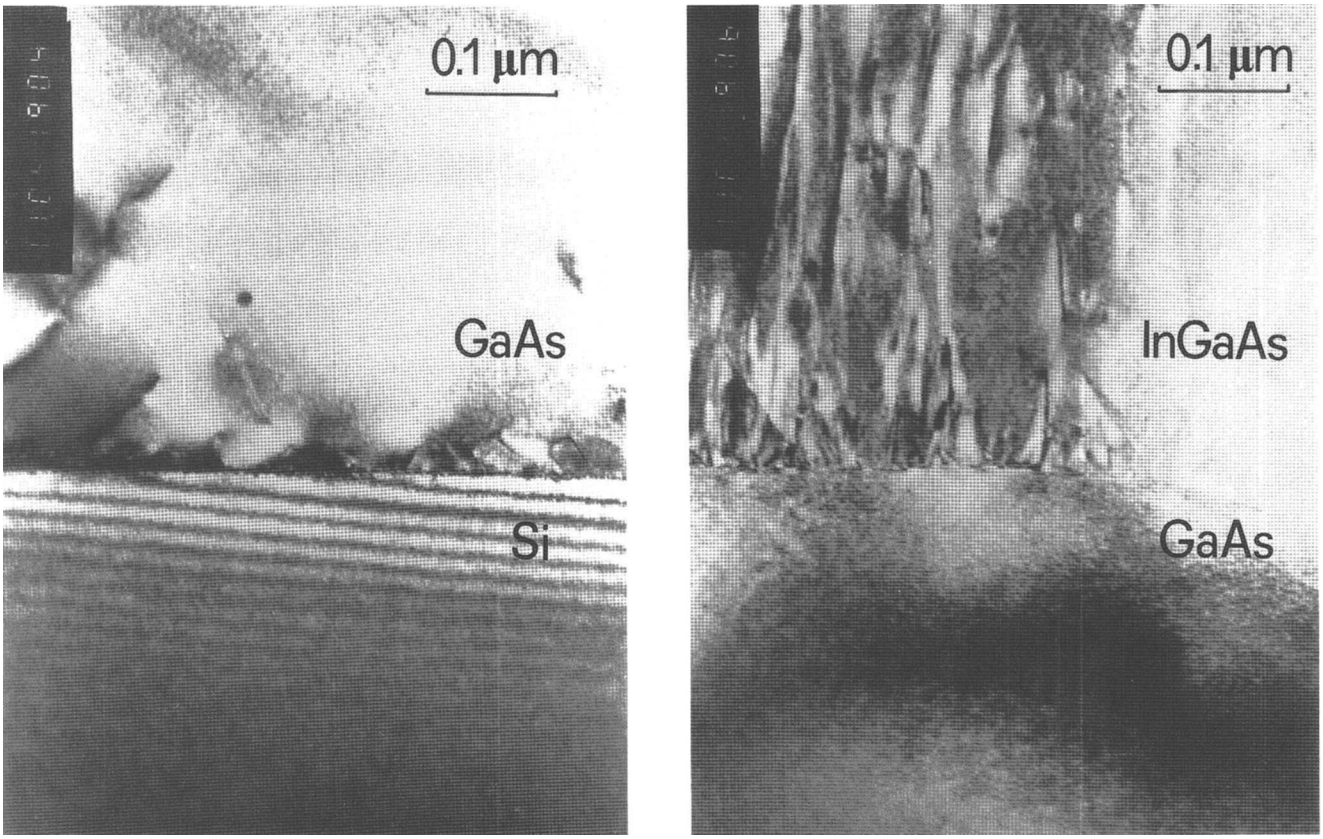

FIG. 5. Higher magnification XTEM micrographs showing (a) the GaAs/Si and (b) the $In_{0.53}Ga_{0.47}As$/GaAs interfaces in sample #7.

in comparison with the other samples shown in Table II and to a highly distorted growth in the InGaAs/GaAs/Si interfacial region [Fig. 8(a)]. Although in the XTEM micrograph of Fig. 8(a) the GaAs/InGaAs interface is not visible, the Transmission Electron Diffraction (TED) patterns exhibit triplet diffraction spots corresponding to the Si, GaAs, and $In_{0.53}Ga_{0.47}As$ crystals [Fig. 8(b)]. This could be explained considering the existence of GaAs islands on Si, separated by InGaAs. Such a severe 3-D growth in the initial stages of sample #1 may explain the higher surface roughness and the observation of highly dislocated islands in the interface [Fig. 8(a)].

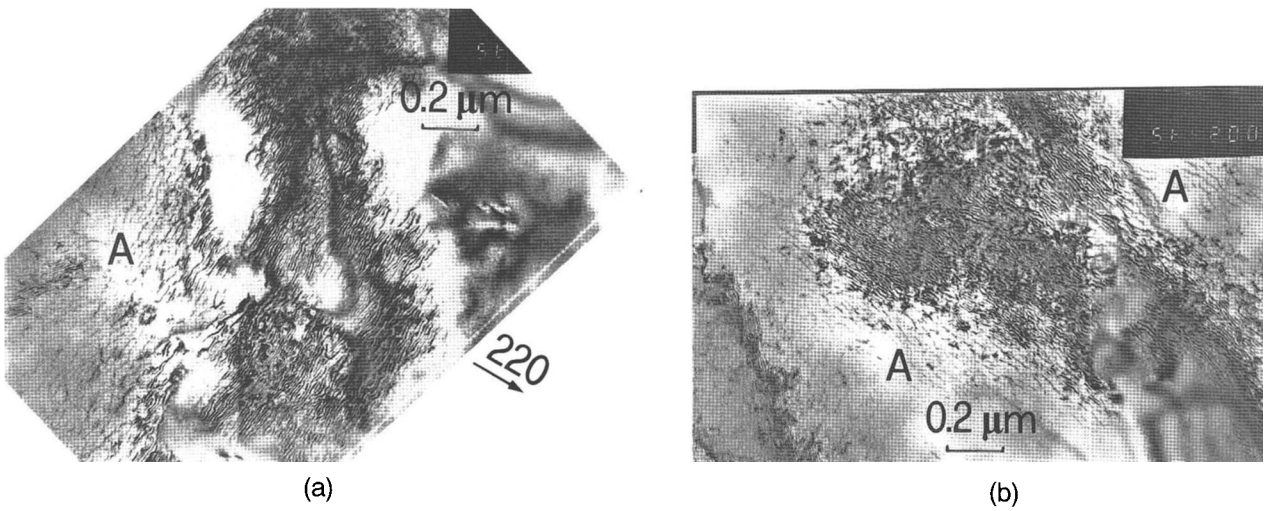

FIG. 6. TEM micrographs from the $In_{0.53}Ga_{0.47}As$/GaAs interfacial region of sample #7, obtained under strong (a) 220 and (b) $2\bar{2}0$ reflections. In the areas marked by the letter A, misfit dislocation segments are visible.

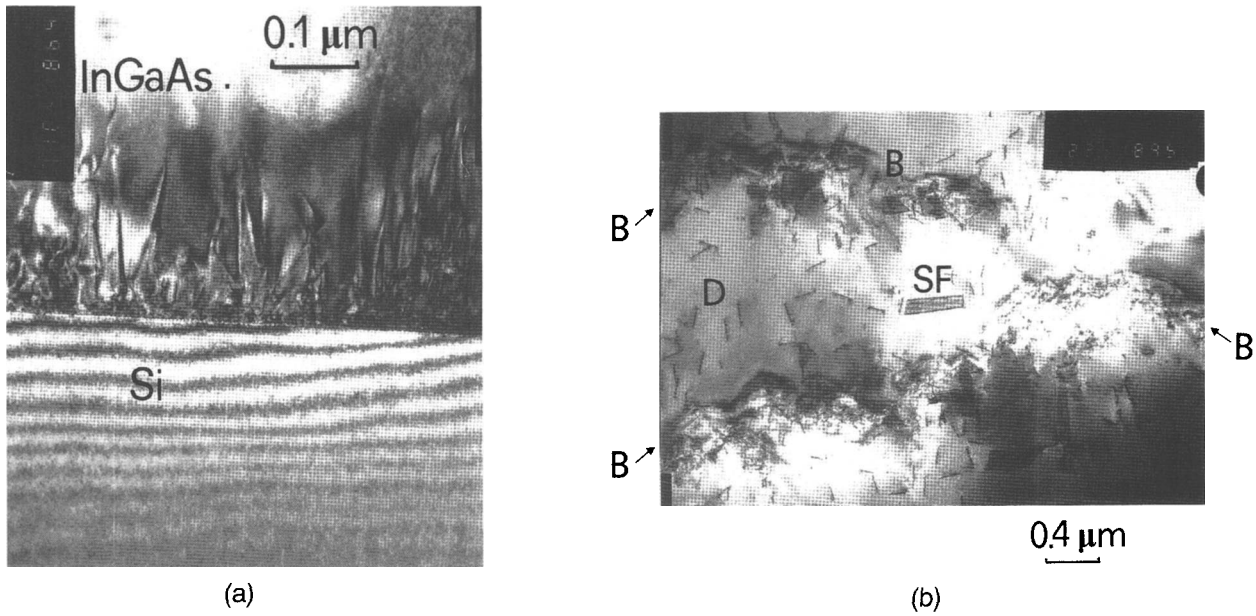

FIG. 7. In sample #12, (a) XTEM micrograph showing the periodic rows of misfit dislocations in the $In_{0.50}Ga_{0.50}As/Si$ interface and (b) TEM micrograph from the $In_{0.53}Ga_{0.47}As$ surface region showing the existence of dislocations (D), stacking faults (SF), and low-angle grain boundaries (B).

Planar view (TEM) observations in sample #9 have shown the higher dislocation density of 8×10^9 cm^{-2} that appeared in the examined samples. Thus, the abruptly graded buffers (types I, II) between GaAs and $In_{0.53}Ga_{0.47}As$ do not improve the InGaAs crystal quality. Sample #14 has shown a lower dislocation density, of

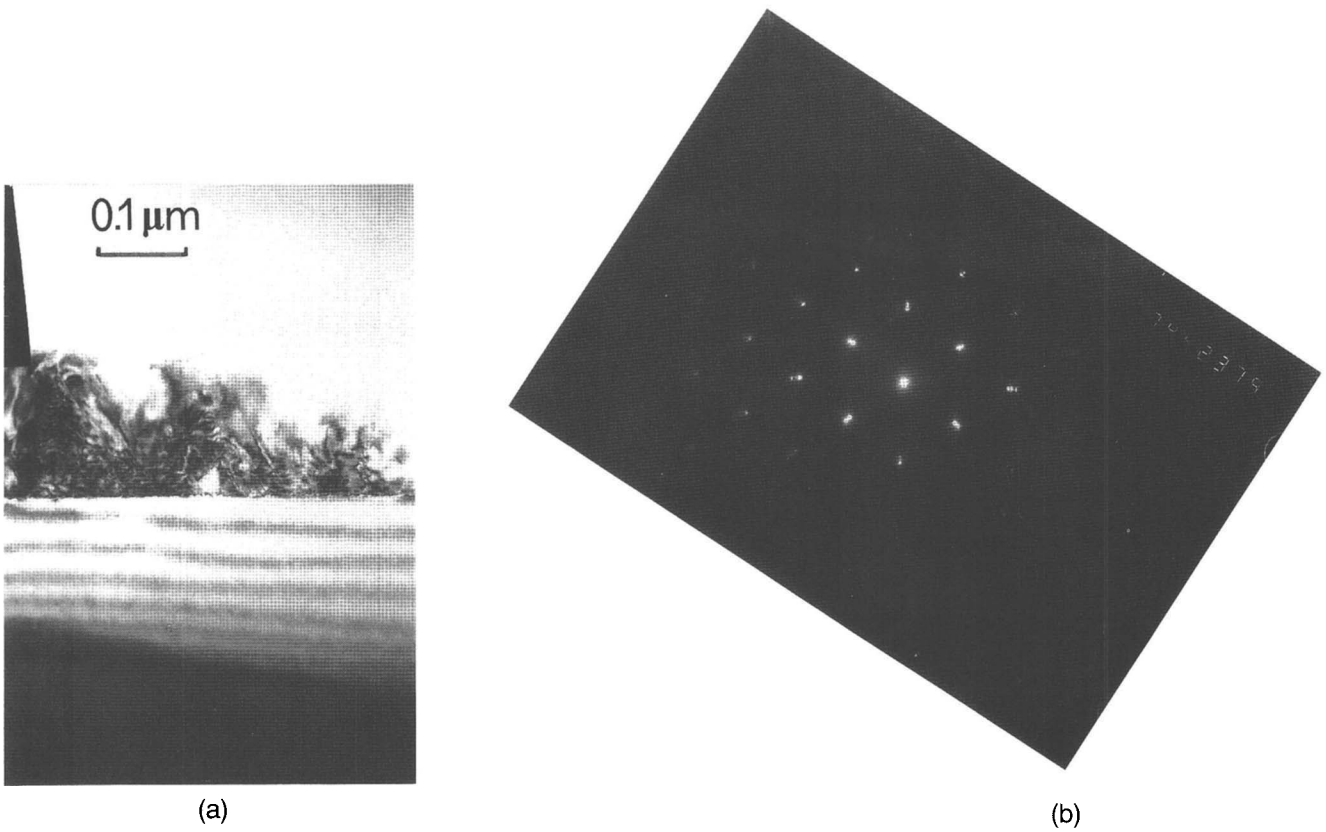

FIG. 8. (a) XTEM micrograph of the $In_{0.53}Ga_{0.47}As$/30 nm GaAs/Si interface for sample #1. (b) In the corresponding TED pattern triplet spots appeared due to Si, GaAs, and $In_{0.53}Ga_{0.47}As$ crystals.

3×10^9 cm^{-2}, near the InGaAs surface, which should be attributed to the high $In_{0.53}Ga_{0.47}As$ thickness of 6 μm. In sample #14 ten periods of (3ML InAs/3ML GaAs) short period strained superlattices have been introduced four times in the $In_{0.53}Ga_{0.47}As$ film, but the XTEM observations have shown that they have no effect on threading dislocation propagation. The totality of the results indicates that a biaxial strain on (001) planes has no effect on the threading dislocations that run almost parallel to the [001] growth axis.

The low-angle grain boundaries have been revealed by planar view (TEM) observations of the $In_{0.53}Ga_{0.47}As$ films [Fig. 7(b)]. Their density was lower in sample #7 and higher in sample #14 (Table II). Sample #14 has also shown the higher density of stacking faults (5×10^7 cm^{-2}) while the lower values were obtained for samples #7 and #12 (3×10^6 and 5×10^6 cm^{-2}, respectively). The correlation of low-angle grain boundary and stacking fault densities indicates that they should be attributed to the same growth problems.

Spinodal decomposition was presented also in the $In_{0.53}Ga_{0.47}As$ films except for #1. Two different scales of contrast were observed for spinodal decomposition. The fine one was observed both in XTEM and TEM micrographs of the samples grown without the GaAs intermediate layer (#12 and 14). In XTEM micrographs this contrast results in very fine bands parallel to the [001] growth direction, of about 10 nm in width, as shown in the micrograph of Fig. 9(a). The fine contrast is more intense at the regions where the dislocation density is lower. It is intense under strong 220 reflection [Fig. 9(a)] while it becomes invisible under (004) reflection that is perpendicular to the substrate [Fig. 9(b)]. Planar view micrographs from sample #12 exhibited fine contrast from spinodal decomposition which, however, is not very intense due to the very high density of dislocations. Stronger intensity fine contrast was observed in TEM micrographs for sample #14 although the contrast scale varied in different areas of this sample. Spinodal decomposition exhibited a coarse-scale contrast in the TEM observations of samples #7, 9, and occasionally for #12. This is clearly evident in the plan view micrograph of Fig. 10(a) where bands of about 100 nm in width run parallel to the [110] direction, which is the vicinal direction of the silicon substrate. The contrast due to spinodal decomposition takes the maximum value when the reflection g is perpendicular to the direction of the lines [Fig. 10(a)]. When the reflection g is parallel to the bands of spinodal decomposition, the fault is invisible [Fig. 10(b)].

The diffraction contrast experiments described above indicate that both the fine- and the coarse-scale contrasts are related to a principal strain in the [110] direction lying parallel to the (001) growth plane. This can be explained by composition modulation in that direction that is produced from spinodal decomposition, in agreement with similar arguments for other III-V ternary or quaternary alloys grown on III-V binary substrates.[19–24] However, the spinodal decomposition in $In_xGa_{1-x}As$ ($x = 0.53$) films grown on vicinal Si substrates is strictly different compared to InGaAs or InGaAsP films grown on GaAs or InP substrates, where decomposition occurs along the [100] and [010] crystallographic directions parallel to the substrate.

IV. DISCUSSION

In our investigation of $In_xGa_{1-x}As$ on Si heteroepitaxy we chose to study the alloy composition around $x = 0.53$. This is probably the extreme case of the

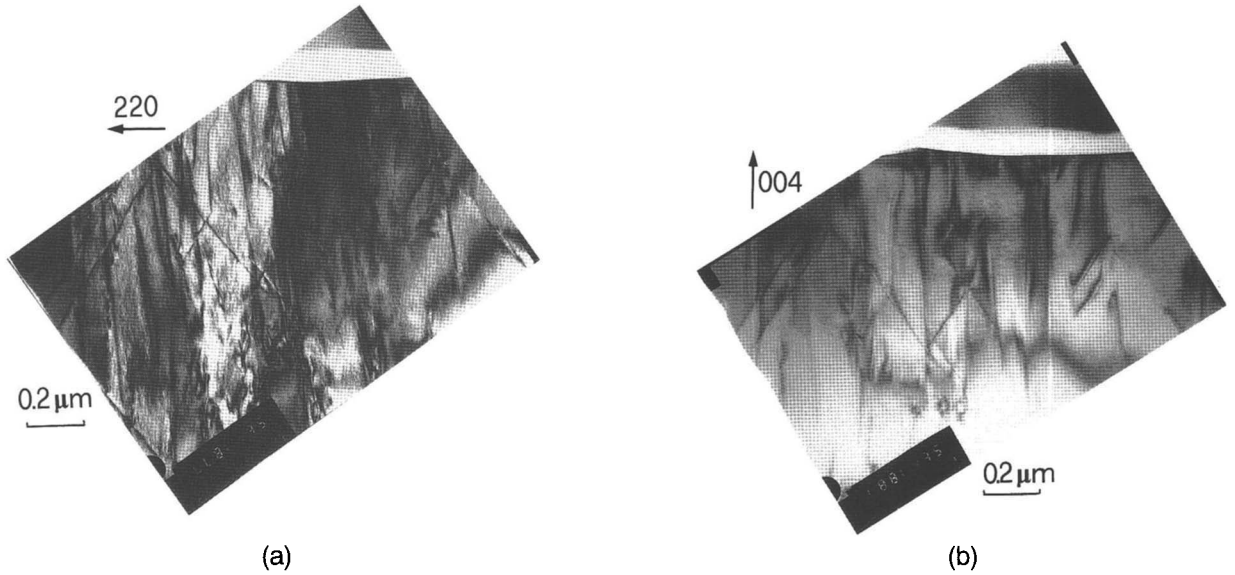

FIG. 9. XTEM micrographs showing the surface region of sample #12. The micrographs were obtained under strong (a) 220 reflection and (b) 004 reflection.

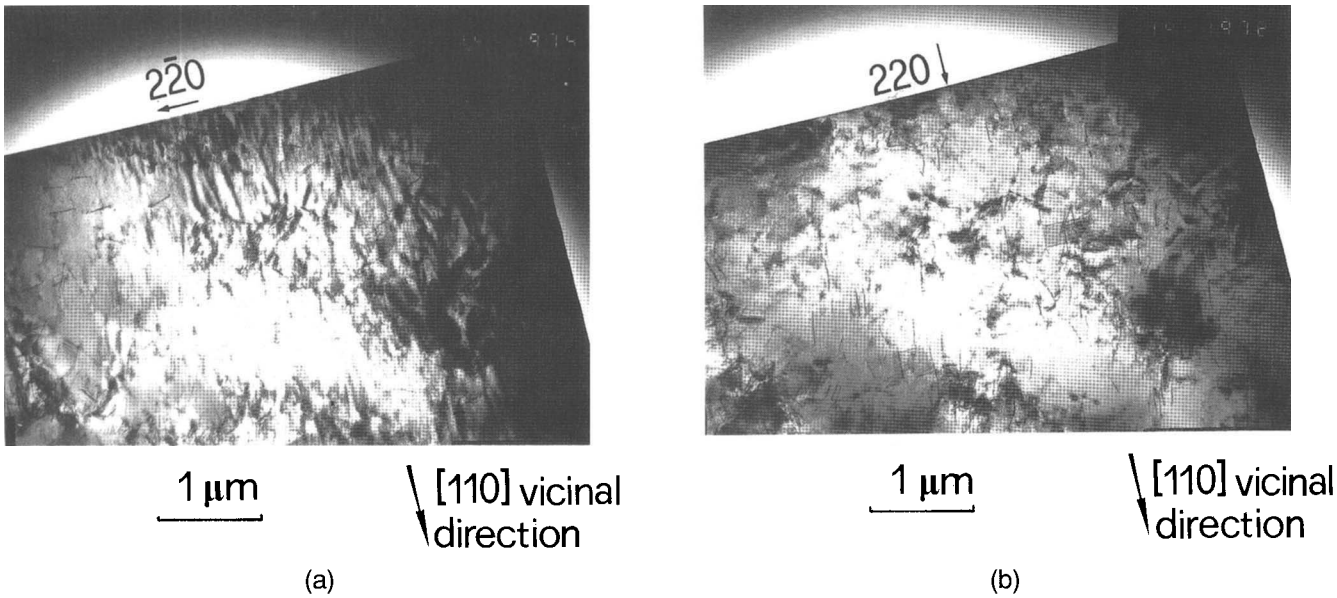

FIG. 10. TEM micrographs for the surface layers of sample #7 taken with different diffraction conditions: (a) the 2$\bar{2}$0 reflection perpendicular to the spinodal bands is strong and (b) the 220 reflection parallel to the spinodal bands is strong.

useful $In_xGa_{1-x}As$ alloy compositions for optical communications, representing the higher misfit values for epitaxy on Si. The $In_{0.53}Ga_{0.47}As$ films showed a crystal structure with a dislocation density of more than one order higher than that obtained in state-of-the-art GaAs on Si,[3] while planar faults and alloy clustering have additionally appeared. These observations cannot be explained by the high misfit value, but they are, rather, related to the specific material properties. The alloy nature is probably relevant to the observed behavior, since the InGaAs or InAlAs growth problems are known to appear even on InP substrates.[33,34] Additionally, for In composition around 0.5 the immiscibility problems are strong,[11] and this may affect the InGaAs growth mode.

The defects appearing in InGaAs on Si are mainly the consequences of a severe 3-D growth mechanism at the early stages of the $In_{0.53}Ga_{0.47}As$ growth on lattice mismatched substrates.[15–18] Following observations in GaAs/Si,[16] it is expected that the InGaAs islands should be slightly misoriented at a magnitude proportional to their individual size. The coalescence of misoriented nuclei results in grain boundaries. Notice that the low-angle grain boundaries are formed only on the InGaAs layers while the intermediate GaAs layers are free of these defects. This shows that the misorientation between InGaAs islands is higher and/or they coalesce at later times, comparing to the first GaAs islands on Si. A phase separation into In-rich and Ga-rich islands during nucleation is also suspected for the above observations. Such a separation may be favored thermodynamically in specific substrates or substrate orientations.[35,36] Since the elastic energy term due to the misfit may be different for islands or continuous films, a different phase separation trend should also be expected for each case.

In contrast to the GaAs on Si, the InGaAs growth mode seems to remain three-dimensional during the entire growth. This is consistent with the rougher surface morphologies and the existence of stacking faults. This type of growth develops {111} facets, and stacking faults are formed due to a wrong accommodation of atoms on these planes.[15]

TABLE II. Defect densities in the surface region of various $In_xGa_{1-x}As$ ($x \sim 0.53$) on silicon samples, as estimated by TEM or XTEM observations.

Sample no.	Roughness (nm)	Dislocations (cm^{-2})	Stacking faults (cm^{-2})	Low-angle grain boundaries (cm^{-2})	Spinodal contrast	Observations
1	75	5×10^9	...	...	No	XTEM
7	50	3×10^9	3×10^6	6×10^6	Coarse	TEM, XTEM
9	...	8×10^9	...	10^7	Coarse	TEM
12	50	7×10^9	5×10^6	2×10^7	Fine	TEM, XTEM
14	35	3×10^9	5×10^7	2×10^7	Varying	TEM, XTEM

The growth of epitaxial Si layers before the InGaAs deposition resulted in better InGaAs crystalline and optical quality which is attributed to the elimination of surface defects[31] and contamination that may appear in the deoxidized surface. On the improved Si surfaces a more homogeneous InGaAs nucleation was accomplished. When the 3-D islands coalesce to form a uniform film, fewer defects are generated, probably since the differences in island orientation are decreased. The island evolution seems also to depend slightly on the misfit value. Thus, the lower defect densities (ignoring spinodal decomposition) appeared for $In_{0.53}Ga_{0.47}As$ grown on the 1.5 μm thick GaAs buffer.

The coarse-scale spinodal decomposition contrast, with period of about 0.1 μm, seems to appear when $In_{0.53}Ga_{0.47}As$ was grown on GaAs/Si or a more closely matched buffer layer (i.e., on $In_{0.44}Ga_{0.56}As$ for sample #9). The fine contrast appears for direct growth on Si. However, when thick films are grown directly on Si both contrast scales are present. These observations are obviously related to the substrate effects on phase separation.[8,10,35,36] A significant new observation concerning InGaAs spinodal decomposition is that the decomposition occurred perpendicular to the [110] vicinal directions of (001) Si and not along the directions [100] and [010], as was reported until today[19–25] for growth on (001) InP or GaAs substrates. The ⟨100⟩ directions in the III-V compounds are the softest directions and thus the spinodal decomposition in bulk crystals should occur preferentially along these directions, since the strain energy term due to composition modulation has a minimum value.[19] Our results highlight the significance of the misfit stresses in the thermodynamic description and stability of lattice-mismatched heteroepitaxial alloy films,[35] since the anisotropic residual strain due to the tilted substrate is probably responsible for the preferential decomposition along one ⟨110⟩ direction. In fact, in the GaAs on Si initial stages of growth (up to ~100 nm), a residual compressive strain anisotropy has been reported.[37]

The spinodal decomposition may be related to the high dislocation densities in InGaAs on Si. Spinodal decomposition also strengthens the matrix, making dislocation glide and climb energetically unfavorable.[20] Thus, comparing GaAs and InGaAs films, different misfit dislocation generation mechanisms should be involved for misfit relaxation. Additionally, any generated threading dislocations in GaAs on Si are mobile under the force of a residual misfit strain which results in glide and a subsequent decrease in their density. In contrast, the threading dislocations in InGaAs on Si are not mobile enough and so their annihilation is less probable. The redistribution of misfit dislocations is also prohibited, thus explaining the observation of 100 nm long misfit dislocation segments.

In conclusion, significant progress has been accomplished in our understanding of the MBE growth of $In_xGa_{1-x}As$ on Si. The growth problems appear to be related to the $In_xGa_{1-x}As$ alloy properties. An extensive further study is needed to address definitely the various growth issues. This would allow for the choice of experimental conditions (i.e., alloy composition, buffer layer, Si orientation), in order to enhance material properties that are required for optoelectronics. The use of Si buffer layers presents one possible approach in that it improves the silicon surface quality and may enhance 2-D nucleation of InGaAs.

V. SUMMARY

In this paper we have presented the systematic study of the $In_{0.53}Ga_{0.47}As$ heteroepitaxy on silicon and have evaluated the material quality for that specific indium composition. Threading dislocations, stacking faults, low-angle grain boundaries, and spinodal decomposition were present in the films. The better crystalline quality (ignoring decomposition) was obtained using a thick GaAs intermediate layer. However, better optical properties were achieved by direct InGaAs deposition on Si. The spinodal decomposition contrast modulation occurred perpendicular to the [110] vicinal direction of the tilted (001) Si substrate which emphasizes the effects that the substrates may have on the thermodynamic description and stability of thin alloy films. The thermodynamically predicted InGaAs trend toward immiscibility results in rough growth fronts during the MBE growth of $In_{0.53}Ga_{0.47}As$ on lattice mismatched substrates. The deviation from a layer-by-layer growth mode results in the generation of the high defect densities present in the InGaAs on Si films. It is necessary to optimize the $In_xGa_{1-x}As$ composition, the buffer layer type, the growth conditions, and the Si orientation, in order to obtain high quality $In_xGa_{1-x}As$ on Si.

ACKNOWLEDGMENTS

This work was supported in part by the European Community under RACE Project 1027. We wish to thank Mr. M. Lagadas for his assistance in MBE growth experiments and Miss K. Tsagaraki for SEM observations.

REFERENCES

1. P. Panayotatos, A. Georgakilas, J-L. Mourrain, and A. Christou, in *Physical Concepts of Materials for Novel Optoelectronic Device Applications I*, edited by M. Raseghi, SPIE **1361** (1990), p. 1100.
2. N.A. Papanicolaou, G.W. Anderson, J.A. Modolo, and A. Georgakilas, Superlattices and Microstructures **8**, 273 (1990).
3. A. Georgakilas, J. Stoemenos, C. Berge, C. Michelakis, C. Cason, M. Lagadas, Z. Hatzopoulos, and A. Christou, in Institute of Physics Conference Series No. **112**, edited by K.E. Singer (1990), p. 135; A. Georgakilas, P. Panayotatos, J. Stoemenos, J-L. Mourrain, and A. Christou, J. Appl. Phys. **71**, 2679 (1992).

4. J. P. Van der Ziel and N. Chand, J. Appl. Phys. **68**, 2731 (1990).
5. A. Dimoulas, P. Tzanetakis, A. Georgakilas, O. J. Glembocki, and A. Christou, J. Appl. Phys. **67**, 4389 (1990).
6. H. Kroemer, in *Heteroepitaxy on Silicon*, edited by J. C. C. Fan and J. M. Poate (Mater. Res. Soc. Symp. Proc. **67**, Pittsburgh, PA, 1986), p. 3.
7. A. Georgakilas, K. Tsagaraki, and A. Christou, Mater. Lett. **10**, 525 (1991).
8. B. de Cremoux, J. Phys. (Paris) **43**, colloq. C5, suppl. no 12, C5-19 (1982).
9. G. B. Stringfellow, J. Cryst. Growth **58**, 194 (1982).
10. F. Glass, J. Appl. Phys. **62**, 3201 (1987).
11. N. Motta, A. Shaukat, A. Qteish, and A. Balzarotti, in Proc. of 20th ICPS, edited by E. M. Anastassakis and J. D. Joannopoulos (World Scientific, 1990), Vol. 3, p. 2625.
12. S-H. Wei, L. G. Ferreira, and A. Zunger, Phys. Rev. B **41**, 8240 (1990).
13. J. W. Mathews, in *Dislocations in Solids*, edited by F. R. N. Nabarro (North-Holland, Amsterdam, 1979), Vol. 2, Chap. 7.
14. J. W. Mathews and A. E. Blakeslee, J. Cryst. Growth **27**, 118 (1974).
15. P. Pirouz, F. Ernst, and T. T. Cheng, in *Heteroepitaxy on Silicon: Fundamentals, Structures, and Devices*, edited by H. K. Choi, R. Hull, H. Ishiwara, and R. J. Nemanich (Mater. Res. Soc. Symp. Proc. **116**, Pittsburgh, PA, 1988), p 57.
16. L. J. Schowalter, in Heteroepitaxy on Silicon: Fundamentals, Structures, and Devices, edited by H. K. Choi, R. Hull, H. Ishiwara, and R. J. Nemanich (Mater. Res. Soc. Symp. Proc. **116**, Pittsburgh, PA, 1988), p. 3.
17. H. L. Tsai and R. J. Matyi, Appl. Phys. Lett. **55**, 265 (1989).
18. M. H. Grabow and G. H. Gilmer, Surf. Sci. **194**, 333 (1988).
19. F. Glas, in *Evaluation of Advanced Semiconductor Materials by Electron Microscopy*, NATO ASI series B, Phys., edited by D. Cherns (Plenum Press, New York, 1989), Vol. 203, p. 217.
20. S. Mahajan and M. A. Shahid, in *Advances in Materials, Processing and Devices in III-V Compound Semiconductors*, edited by D. K. Sadana, L. E. Eastman, and R. Dupuis (Mater. Res. Soc. Symp. Proc. **144**, Pittsburgh, PA, 1989), p. 169.
21. F. Peiró, A. Cornet, J. R. Morante, S. Clark, and R. H. Williams, Appl. Phys. Lett. **59**, 1957 (1991).
22. J. P. Gowers, Appl. Phys. A **31**, 23 (1983).
23. P. Hénoc, A. Izrael, M. Quillec, and H. Launois, Appl. Phys. Lett. **40**, 963 (1982).
24. S. N. G. Chu, S. Nakahara, K. E. Strege, and W. D. Johnston, Jr., J. Appl. Phys. **57**, 4610 (1985).
25. R. A. D. Mackenzie, J. A. Liddle, and C. R. M. Grovenor, J. Appl. Phys. **69**, 250 (1991).
26. M. K. Lee, D. S. Wuu, and H. H. Tung, Appl. Phys. Lett. **50**, 1725 (1987).
27. M. Razeghi, M. Defour, R. Blondeau, F. Omnes, P. Maurel, O. Acher, F. Brillouet, J. C. C. Fan, and J. Salerno, Appl. Phys. Lett. **53**, 2389 (1988).
28. K. Oe and H. Takeuchi, Jpn. J. Appl. Phys. **26**, L120 (1987).
29. A. Georgakilas, Z. Hatzopoulos, A. A. Iliadis, and A. Christou, Mater. Lett. **7**, 456 (1989).
30. K. Kugimiya, Y. Hirofuji, and N. Matsuo, Jpn. J. Appl. Phys. **24**, 564 (1985).
31. R. Hull, A. Fischer-Colbrie, and S. J. Rosner, Appl. Phys. Lett. **51**, 1723 (1987).
32. A. Georgakilas, M. Lagadas, J. Stoemenos, and A. Christou, presented in sixth Europ. Conf. on MBE and Relat. Growth Methods, April 21–24, Tampere, Finland, 1991.
33. J. P. Praseuth, L. Goldstein, P. Hénoc, J. Primot, and G. Danan, J. Appl. Phys. **61**, 215 (1987).
34. A. Salokatve and M. Hovinen, J. Appl. Phys. **67**, 3378 (1990).
35. W. C. Johnson and C. S. Chiang, J. Appl. Phys. **64**, 1155 (1988).
36. F. C. Larché, W. C. Johnson, C. S. Chiang, and G. Martin, J. Appl. Phys. **64**, 5251 (1988).
37. S. M. Koch, S. J. Rosner, R. Hull, G. W. Voffe, and J. S. Harris, Jr., J. Cryst. Growth **81**, 205 (1987).